

Article

# Iron Transport across Brain Barriers: Model and Numerical Parameter Estimation

Eleonora Ficiara <sup>\*,†</sup> , Ilaria Stura <sup>†</sup> and Caterina Guiot 

Department of Neurosciences, University of Turin, 10124 Turin, Italy

\* Correspondence: [eleonora.ficiara@unito.it](mailto:eleonora.ficiara@unito.it)

† These authors contributed equally to this work.

**Abstract:** Iron is an essential element for brain metabolism. However, its imbalance and accumulation are implicated in the processes featuring neurodegenerative diseases, such as Alzheimer's disease (AD). The brain barrier's system maintains the sensitive homeostasis of iron in the brain. However, the impairment of the mechanisms of iron passage across the brain barrier is not clearly established. A mathematical model is proposed to macroscopically describe the iron exchange between blood and cerebral compartments. Numerical simulations are performed to reproduce biological values of iron levels in physiological and pathological conditions. Moreover, given different scenarios (neurological control and AD patients), a particle swarm optimization (PSO) algorithm is applied to estimate the parameters. This reverse work could be important to allow the understanding of the patient's scenario. The presented mathematical model can therefore guide new experiments, highlighting further dysregulated mechanisms involved in neurodegeneration as well as the novel disease-modifying therapies counteracting the progression of neurodegenerative diseases.

**Keywords:** compartmental model; iron; optimization

MSC: 92; 92b05



**Citation:** Ficiara, E.; Stura, I.; Guiot, C. Iron Transport across Brain Barriers: Model and Numerical Parameter Estimation. *Mathematics* **2022**, *10*, 4461. <https://doi.org/10.3390/math10234461>

Academic Editor: Sergei Petrovskii

Received: 4 November 2022

Accepted: 24 November 2022

Published: 26 November 2022

**Publisher's Note:** MDPI stays neutral with regard to jurisdictional claims in published maps and institutional affiliations.



**Copyright:** © 2022 by the authors. Licensee MDPI, Basel, Switzerland. This article is an open access article distributed under the terms and conditions of the Creative Commons Attribution (CC BY) license (<https://creativecommons.org/licenses/by/4.0/>).

## 1. Introduction

### 1.1. Biological Background

Iron is an essential element for brain functions, but iron accumulation can induce oxidative stress and consequent neurotoxicity. Recent studies revealed a role of iron in neurodegenerative diseases [1–3] and in age-related cognitive decline [4]. However, contrasting results are present in the literature about iron and iron-related protein levels in biological fluids. Furthermore, the understanding of the mechanisms for brain iron import/export is still limited, requiring further investigation.

The sensitive balance of iron levels in the central nervous system (CNS) is mainly maintained by the brain barriers system, coordinating an efficient transport and recycling in the brain. Impairments in iron influx/efflux mechanisms at brain barrier interfaces can contribute to altered levels of iron in cerebrospinal fluid (CSF) and brain tissue, leading to pathological conditions.

Blood iron entrance in the brain is controlled by the blood–brain barrier (BBB) [5] and, to a lesser extent, by the blood–cerebrospinal fluid barrier (BCSFB) [6]. The BBB is a highly selective barrier, composed of endothelial cells with specialized tight junctions, separating blood from brain.

The BCSFB separates the systemic circulation from the CSF, filling the cerebral spaces. The CSF is produced and finely controlled by the choroid plexus (CP) located in the ventricles, and it is strictly in contact with the CNS, exchanging relevant compounds, including metals. Beyond the restriction of the access of substances from blood to CSF, the BCSFB is known to remove substances from the CSF to the blood [7]. It is reported that

metals such as iron and copper may influx in the interstitial fluid (ISF) of the brain via BBB and be transported back into the blood via the efflux mechanism at the BCSFB, removing substances from the CSF circulation [8].

Materials in the CSF and in the brain ISF can freely exchange, in a bidirectional way, due to the lack of structural barrier between these two fluid compartments [9].

Since CSF collects waste substances from the brain, it is important to consider the role of CSF–ISF exchange, linked to the efflux and clearance of interstitial solutes. Growing interest is aimed at the glymphatic system, a brain-wide network of perivascular pathways supporting the exchange of CSF and ISF and contributing to clearing waste in the brain [10].

The temporal dynamic of iron exchange from blood to brain affects both influx and efflux rates. The iron content in the brain depends on aging [11] and it was shown that an imbalance of iron influx and efflux causes brain iron accumulation over time in the healthy adult rat [12].

### 1.2. Previous Mathematical Models

The mammalian organism maintains a complex network to regulate iron uptake, excretion, and distribution into the organs. Theoretical models aiming to describe iron metabolism are present in the literature [13–15]. For example, Lopes et al. presented a kinematic model of the dynamic system of iron pools and fluxes, reflecting systemic properties of iron metabolism [13]. Based on systematic measurements, quantitative values of rate constants for the iron flux from plasma into 15 peripheral organs of the body were estimated, evaluating the kinematic properties of iron-containing compartments, such as hierarchy of iron residence times and iron distribution in different organs [13]. Furthermore, focusing on the iron exchange from blood to brain, ordinary differential equations were formulated based on the first-order reaction kinetics to model the iron transport, effectively reproducing the experimental data of iron through BBB endothelial cells for many in vitro studies [16].

Under the hypothesis that imbalance in iron transport mechanisms at the BCSFB and/or BBB can be a factor for the elevated iron levels in the brain, we developed two mathematical models to macroscopically describe the passage of iron from blood to brain environment and its potential alteration in neurodegenerative conditions [17,18]. Starting from experimental measurements and literature data for the parameters estimation, we sequentially proposed a two-compartmental model (blood and CSF compartments) [17] and a three-compartmental model, implementing the previous one with the addition of the brain ISF compartment [18]. These models can simulate the iron concentrations found in biofluids in different conditions (such as dementia, and neurological controls).

However, our models need to be supported by ad hoc experimental data (i.e., longitudinal data and/or specific measurements in brain ISF) for a more realistic and accurate estimation of the parameters. Then, the uncertainty of the parameters due to high intrinsic biological variability of iron measurements requires future experimental data to set the range of the parameters more precisely, for a better discrimination between physiological and pathological condition.

### 1.3. Aim of the Work

In order to improve the limitations of our previous models, the aim of this work is to test the robustness of the proposed three-compartmental model for iron transport, exploiting an optimization algorithm to estimate the parameters. The parameters estimation will show if the model is able to macroscopically describe the passage of iron across blood and brain environment in different scenarios, i.e., in physiological and pathological conditions.

## 2. Methods

### 2.1. Mathematical Model

A three-compartmental model based on a nonhomogeneous system of first-order ordinary differential equations (ODEs), described by (1), (2), and (3), was used to simulate the passage of iron from blood to the brain.

$$\begin{cases} \frac{dI_B}{d\tau} = -(a_{12} + k)I_B + \alpha_{21} I_{CSF} - b_{13} I_B + b_{31} I_{ISF} + E & (1) \\ \frac{dI_{CSF}}{d\tau} = a_{12} I_B - (\alpha_{21} + a_{23})I_{CSF} + a_{32} I_{ISF} & (2) \\ \frac{dI_{ISF}}{d\tau} = b_{13} I_B + a_{23} I_{CSF} - (a_{32} + b_{31})I_{ISF} & (3) \end{cases}$$

The three compartments describe the blood, the CSF, and the ISF surrounding the brain. The variables describe the iron concentration in blood ( $I_B$ ), CSF ( $I_{CSF}$ ), and ISF ( $I_{ISF}$ ), respectively, expressed in mg/L. For more details on the equation terms, see [17,18]. The parameter values are summarized in Table 1. These values were estimated based on the literature, as explained in previous works [17,18].

**Table 1.** Description and value of parameters used for the equations.

Parameter	Description	Normal Value	High Rate Value
E	Iron intake into the blood from food (mg/L)	0.22	0.22
k	Iron consumption from blood and excretion mechanisms	0.23	0.23
$a_{12}$	Kinetic constant rate for iron entering from blood to CSF across BCSFB	0.0002	0.001
$\alpha_{21}$	Kinetic constant rate for iron returning from CSF and brain to blood	0.05	0.08
$a_{23}$	Kinetic constant rate for iron passing from CSF to ISF	0.8	0.8
$a_{32}$	Kinetic constant rate for iron passing from ISF to CSF	1	1
$b_{13}$	Kinetic constant rate for iron entering from blood to brain (consequently ISF), across BBB	0.002	0.005
$b_{31}$	Kinetic constant rate for iron returning from the brain to blood	$1 \times 10^{-6}$	$5 \times 10^{-6}$

Sensitivity analysis was performed to rank the relevance of the parameters based on potential ranges of variations [18]. Global sensitivity analysis (GSA) investigates the variations in the model output when all parameters can vary simultaneously over specified ranges. Noninfluential parameters are supposed to be fixed at any value within the range of variability without significantly affecting the model response. Different methods of GSA were previously used on this model and described in [18].

The estimation for iron levels in the compartments is based on iron data from a population of patients affected by different forms of dementia and neurological control [18,19] and on the biological structures described in the introduction.

We hypothesized different values for the parameters according to physiological or pathological conditions. Starting from different initial conditions, numerical simulations were performed [18].

### 2.2. Parameters Estimation

In order to estimate the robustness of the model, parameters estimation is performed. Indeed, in a robust model the estimated parameters will be similar to the chosen ones (see Table 1). Mathematically, the problem consists of finding the minimum of the norm:

$$\|y_t - Y_t\|^2 \tag{4}$$

where  $t$  is the discretization in time of the measures,  $y_t$  are the real data at each time,  $t$ , and  $Y_t$  is the output model, with unknown parameters, at time  $t$ . The minimum of (4), indeed, is the point in the parameters' space  $D$  in which the model is closer to real data, i.e., the point of which coordinates are the chosen model's parameters.

To solve such a problem, the cooperative method called particle swarm optimization (PSO) is chosen. It is based on the mutual interaction and exchange of information between individuals of a swarm (e.g., birds or bees) and it was introduced by Kennedy (social psychologist) and Eberhart (electrical engineer) [20].

Let us consider a group of particles (or birds) which are represented as points in the space  $D$ . Each particle tries to find the place with the maximum availability of food, i.e., the minimum, balancing its own experience (or selfish behavior, which is the ability of the particle to randomly fly away from the swarm to reach the food) with the shared experience of the other particles (social behavior, which is the ability of the bird to stay in the group). When a good trade-off between the two behaviors is reached, the swarm gradually changes its direction until reaching the best "place", i.e., the minimum of the norm.

Formally, each particle has a velocity  $v_i^j$  and a position  $p_i^j$ , where  $j = 1, \dots, N_{max}$  is the iteration number and  $i = 1, \dots, n$  is the bird's index. Initially, the  $n$  particles are randomly initialized in the search-space  $D$  with random initial velocities and positions. Then, directions and velocities gradually change when each individual moves to the best previous position of itself or of other birds, searching in a neighborhood for a better position, accordingly with these formulas [21,22]:

$$v_i^j = \omega^j v_i^{j-1} + \phi_l^j (l_i^{j-1} - p_i^{j-1}) + \phi_g^j (g_i^{j-1} - p_i^{j-1}) \tag{5}$$

$$p_i^j = \omega^j p_i^{j-1} + v_i^j \tag{6}$$

where  $l_i^{j-1}$  is the previous local best position,  $g_i^{j-1}$  is the previous global best position,  $\omega^j$  is the inertia weight, and  $\phi_l^j, \phi_g^j$  are the cognitive and social components.

Moreover, multiple runs of this algorithm are implemented in order to choose, as final solution, the best one (i.e., the one with minimum (4)). In particular, 10 runs were established to estimate one parameter, while 30 runs were established to estimate two or more parameters.

As  $y_t$ , the output of a model with fixed parameters is used. Finally, in order to test the robustness of the algorithm, white noise ( $\sigma = 0.001, 0.01$ ) is also added at input data. Indeed, the perturbed data should simulate biological observations that can contain errors and variability.

### 3. Results

Based on the results of the sensitivity analysis and on the biological assumptions reported in [18], we focused our work on the parameters  $a_{21}, a_{23}, a_{32}, b_{13}$ . Simulations of both normal and hypothesized pathological conditions were performed, using the parameters values listed in Table 1.

Starting from random initial conditions, numerical simulations were performed, showing that the model is able to simulate the biological values of iron concentration in CSF (Figure 1).

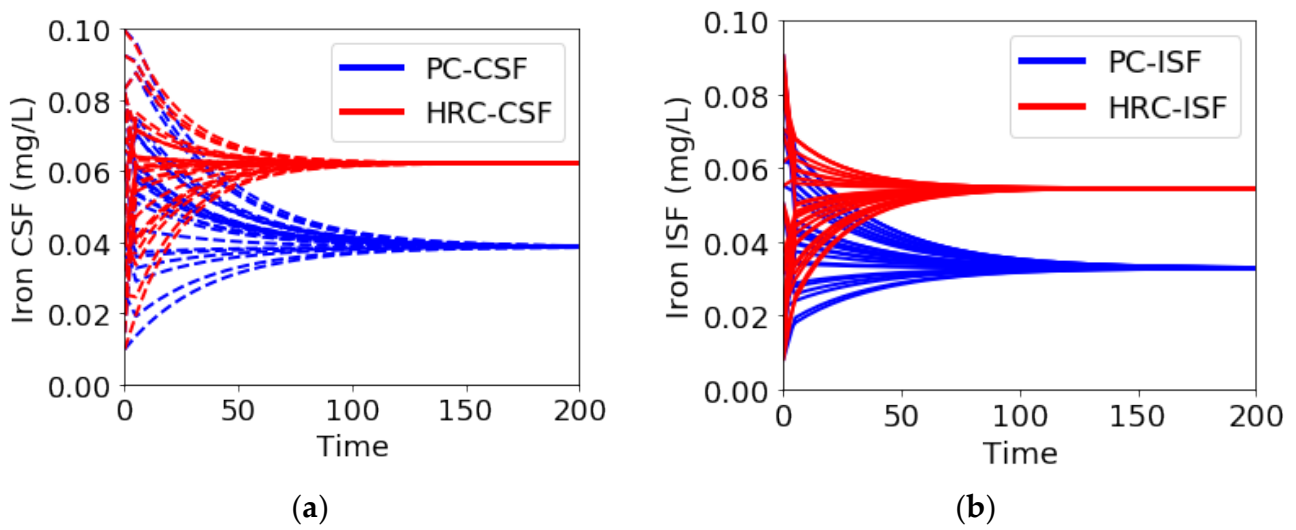


**Figure 1.** Numerical simulations of iron concentration (mg/L) in CSF  $I_{CSF}$  (a) and ISF  $I_{ISF}$  (b) starting from random initial conditions. CSF: cerebrospinal fluid; ISF: interstitial fluid; PC: physiological condition; HRC: high rate condition.

In Table 2, the results of multiple runs of the PSO algorithm are summarized. In particular, two set of parameters were used (normal and high rate) with different random noise ( $\sigma = 0.001, 0.01$ ). The mean error of (4) is reported. In the next subsections, the results are detailed for each number of estimated parameters.

3.1. Estimation of One Parameter

The algorithm works very well in estimating one parameter. The worst performance is given by the parameter  $b_{13}$ , probably because its value is smaller than the other parameters. Without noise on input data, the error at each run is negligible, i.e., only one run is necessary to estimate the parameter. With white noise, in only a few cases the run gives a high error; ten runs for each parameter are sufficient to estimate the correct value.

**Table 2.** Results of parameters’ estimation with PSO, considering one, two, and three parameters estimated at each time, with different noise. PC: physiological condition; HRC: high rate condition.

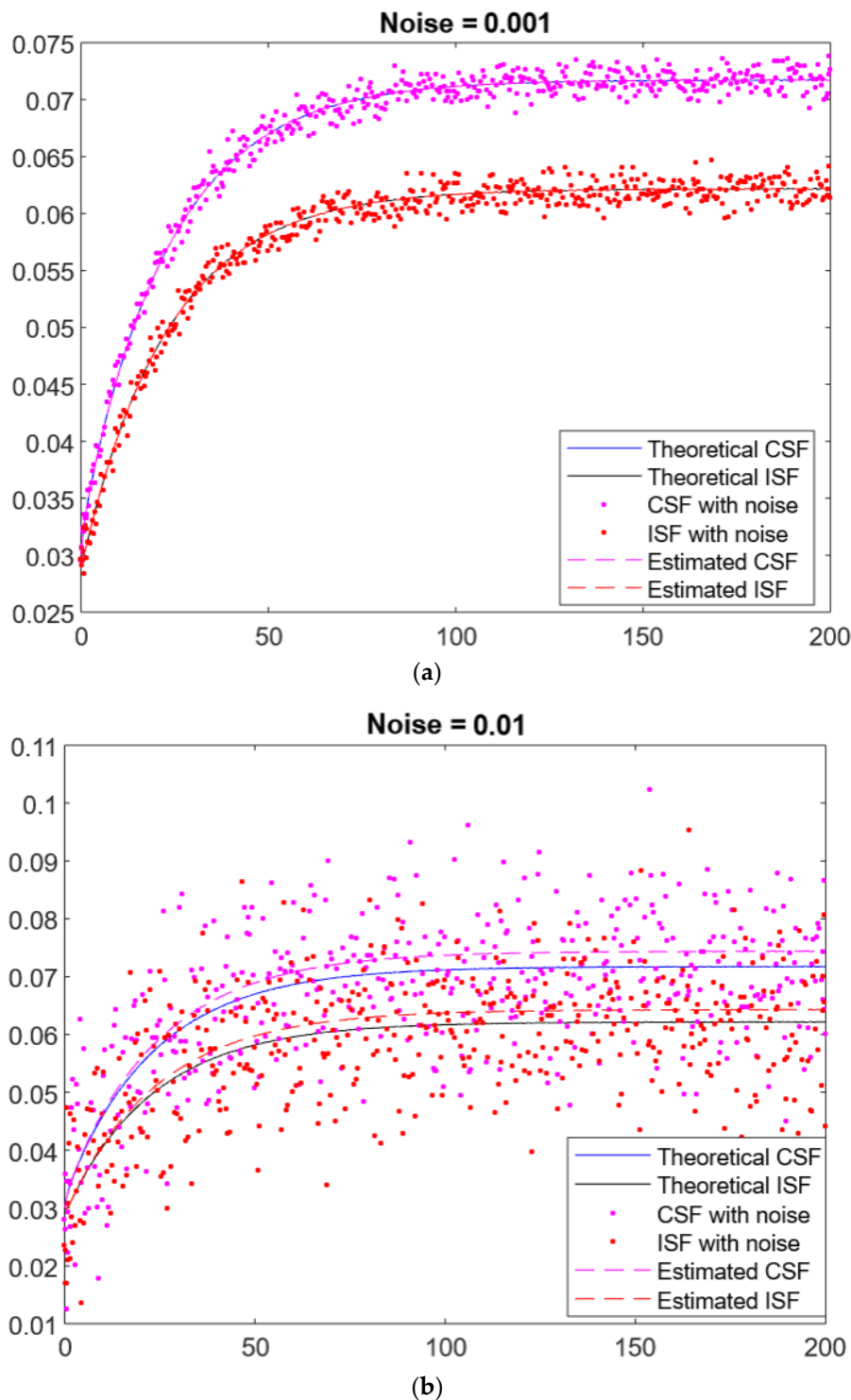
N° of Estimated Parameters	Noise	Parameter	Estimation for PC	Mean Error in PC $\ y_t - Y_t\ ^2$	Estimation for HRC	Mean Error in HRC $\ y_t - Y_t\ ^2$
1	0	$\alpha_{21}$	0.0500	$4.2689 \times 10^{-15}$	0.0800	$3.8223 \times 10^{-15}$
		$a_{32}$	1.0000	$1.1465 \times 10^{-15}$	1.0000	$7.0460 \times 10^{-13}$
		$a_{23}$	0.8000	$2.3891 \times 10^{-11}$	0.8000	$8.4539 \times 10^{-15}$
		$b_{13}$	0.0020	0.6540	0.0050	0.9318
	0.001	$\alpha_{21}$	0.0501	$5.8056 \times 10^{-6}$	0.0799	$1.9159 \times 10^{-6}$
		$a_{32}$	1.0014	$1.2567 \times 10^{-6}$	1.0041	$2.8066 \times 10^{-5}$
		$a_{23}$	0.7926	$3.5431 \times 10^{-5}$	0.7977	$1.0568 \times 10^{-5}$
		$b_{13}$	0.0020	0.5723	0.0050	0.4659
	0.01	$\alpha_{21}$	0.0491	$4.9117 \times 10^{-4}$	0.0818	0.0011
		$a_{32}$	0.9356	0.0023	0.9647	0.0019
		$a_{23}$	0.7457	0.0024	0.7780	0.0010
		$b_{13}$	0.0020	0.4909	0.0050	0.9318

Table 2. Cont.

N° of Estimated Parameters	Noise	Parameter	Estimation for PC	Mean Error in PC $\ y_t - Y_t\ ^2$	Estimation for HRC	Mean Error in HRC $\ y_t - Y_t\ ^2$
2	0	$\alpha_{21}$	0.0500	$3.3379 \times 10^{-14}$	0.0800	$7.9000 \times 10^{-15}$
		$a_{32}$	1.0000		1.0000	
		$\alpha_{21}$	0.0500	$3.4623 \times 10^{-15}$	0.0800	$1.2001 \times 10^{-4}$
		$a_{23}$	0.8000		0.8000	
		$a_{23}$	0.8000	0.0079	0.5998	0.0013
	$a_{32}$	1.0000	0.7692			
	$\alpha_{21}$	0.0930	0.0542	0.0800	0.0428	
	$b_{13}$	0.0037		0.0050		
	$a_{32}$	1.0000	0.3967	0.9909	0.5573	
	$b_{13}$	0.0020		0.0050		
	0.001	$\alpha_{21}$	0.0503	$3.5199 \times 10^{-5}$	0.0800	$1.2536 \times 10^{-5}$
		$a_{32}$	0.9900		1.0007	
		$\alpha_{21}$	0.0499	$5.0687 \times 10^{-6}$	0.0798	$1.0124 \times 10^{-5}$
		$a_{23}$	0.7968		0.7967	
		$a_{23}$	0.0865	0.0324	0.6639	0.2220
$a_{32}$	0.1594	0.8440				
$\alpha_{21}$	0.0503	0.2401	0.0861	0.1399		
$b_{13}$	0.0020		0.0054			
$a_{32}$	1.0223	0.1548	0.9963	0.5516		
$b_{13}$	0.0020		0.0050			
0.01	$\alpha_{21}$	0.0530	0.0052	0.0824	0.0044	
	$a_{32}$	0.9310		0.9339		
	$\alpha_{21}$	0.0505	0.0232	0.0791	0.1628	
	$a_{23}$	0.7411		0.7824		
	$a_{23}$	0.0036	$1.0892 \times 10^{-4}$	0.0767	$5.0163 \times 10^{-4}$	
$a_{32}$	0.0610	0.1621				
$\alpha_{21}$	0.1105	0.1275	0.0850	0.0238		
$b_{13}$	0.0043		0.0053			
$a_{32}$	0.8054	0.2116	0.9838	0.4631		
$b_{13}$	0.0019		0.0049			
3	0	$\alpha_{21}$	1.4080	$6.4164 \times 10^{-4}$	1.5710	0.0920
		$a_{32}$	2.6049		2.7064	
		$b_{13}$	0.0620		0.1121	
		$\alpha_{21}$	0.0500	0.1364	0.0800	0.0157
		$a_{32}$	1.2887		0.9199	
	$a_{23}$	1.0443	0.7302			
	0.001	$\alpha_{21}$	0.8329	41.6743	0.6466	0.1379
		$a_{32}$	1.9264		1.6499	
		$b_{13}$	0.0366		0.0459	
	$\alpha_{21}$	0.0500	$4.5772 \times 10^{-5}$	0.0799	0.4450	
	$a_{32}$	1.3334		0.3549		
	$a_{23}$	1.0806		0.2391		
	0.01	$\alpha_{21}$	1.9090	9.6464	1.0405	0.0699
		$a_{32}$	3.1090		2.0884	
		$b_{13}$	0.0844		0.0743	
$\alpha_{21}$		0.0486	0.0030	0.0809	0.5067	
$a_{32}$		0.1231		2.2613		
$a_{23}$	0.0451	1.9322				

### 3.2. Estimation of Two Parameters

In addition, two parameters are well estimated by PSO. A less performant result is given for the couple  $\alpha_{21}$  and  $b_{13}$ . However, as shown in Figure 2, the reconstructed curves (dotted lines) are similar to the theoretical ones (straight lines with noise  $\sigma = 0.001, 0.01$ ). In general, the estimation of  $b_{13}$  remains problematic due to its very low value.



**Figure 2.** Example of estimation of two parameters ( $\alpha_{21}$  and  $b_{13}$ ) with (a)  $\sigma = 0.001$  and (b)  $\sigma = 0.01$ . Straight lines are the theoretical curves calculated by ode45; dots are the perturbed data in input to PSO; trait lines are the curves estimated by PSO.

### 3.3. Estimation of Three Parameters

The presence of the parameter  $b_{13}$  in the estimation set gives bad results. The simulated parameters, in fact, are out of the expected natural range. This is due to the differences in order between  $b_{13}$  and the other parameters. Indeed, PSO estimates very well the set  $(\alpha_{21}, a_{32}, a_{23})$  with no noise. Worse results are present in the case of high random noise.

## 4. Discussion

In this work we presented a method to explore the robustness of the theoretical model proposed for the iron trafficking across brain barriers. The PSO method was used because it is also very robust in the case of few and sparse data, in combination with enrichment techniques such as radial basis functions [23]. Its usage is known in many fields and it is considered a standard for resolving complex optimization such as image reconstruction [24]. Moreover, the advantages of this method are that it does not require any strong assumptions and it more robust than other deterministic methods [25,26], also in presence of multiple local minima.

In our previous paper, the sensitivity analysis showed that the variation of the three parameters, on which we focused this paper, had a strong impact on the behavior of the model [18]. In our simulations, the parameters  $\alpha_{21}$  and  $b_{13}$  were hypothesized with slight changes between the normal and high rate condition. On the contrary, the values of  $a_{32}$  and  $a_{23}$  were considered the same in both conditions. However, in future works different values could be tested.

These preliminary results show that a good estimation of the parameters from perturbed data (simulating real data) is possible, especially considering the estimation of one or two parameters with 0 or 0.001 of noise added to input data (see Table 2). The parameter  $b_{13}$  seems to be the most problematic in the estimation. From the sensitivity analysis, the variations of this parameter showed a higher contribution on the modulation of iron concentrations in ISF and CSF, especially in the hypothesized pathological condition.

The estimation of three parameters has to be improved. It can be due to the high number of parameters and consequent higher complexity of the model. However, by choosing two parameters with no or moderate noise, a good estimation was obtained. This allows to consider a further step including real longitudinal data of iron concentrations for the parameter estimation from this compartmental model.

The results of the predictions showed some limitations of the model. Firstly, the model needs to be supported by ad hoc experimental and longitudinal data for a more accurate estimation of the parameters set. Future experimental data (for the three compartments: blood, CSF, and brain) can contribute to confirm the simulated dynamic and to set the range of the variability more precisely.

Further implementations should take into account additional factors, such as the time dependence of the parameters and potential correlations between them. In fact, there is evidence for an accumulation of iron with aging [27], especially in several brain regions [28]. In addition, it was reported that a change in the brain iron accumulation rate suggests different brain iron dynamics, including import/export of iron over the course of life [12].

Finally, the compartmental model could be extended to other biomarkers of neurodegenerative diseases, i.e., to investigate the transport of Amyloid-beta and Tau proteins, the well-established hallmarks of AD. In fact, other factors that play a fundamental role in the disease progression, such as proteins and transporters of brain membranes, i.e., ABC transporters [29], can be investigated by in silico models.

## 5. Conclusions

This work is a further step in setting an optimal model of iron transport across the brain barriers, which will help to understand the role of different factors of the process in the AD context. In this paper we presented a method to estimate, in a robust way, the biological parameters based on real data.

The final target of our research is, indeed, to help innovative and personalized in silico therapeutic approaches, such as those based on iron chelation.

**Author Contributions:** Conceptualization, E.F., I.S. and C.G.; methodology, E.F. and I.S.; data curation, E.F. and I.S.; writing—original draft preparation, E.F. and I.S.; writing—review and editing, E.F., I.S. and C.G.; supervision, C.G. All authors have read and agreed to the published version of the manuscript.

**Funding:** Ex-post grant 2020 (GUIC\_S1921\_EX-POST\_21\_01) from University of Torino and Compagnia di San Paolo.

**Data Availability Statement:** The data presented in this study are available on request from the corresponding author.

**Conflicts of Interest:** The authors declare no conflict of interest.

## References

1. Ndayisaba, A.; Kaindlstorfer, C.; Wenning, G.K. Iron in Neurodegeneration—Cause or Consequence? *Front. Neurosci.* **2019**, *13*, 180. [[CrossRef](#)] [[PubMed](#)]
2. Ashraf, A.; So, P.-W. Spotlight on Ferroptosis: Iron-Dependent Cell Death in Alzheimer’s Disease. *Front. Aging Neurosci.* **2020**, *12*, 196. [[CrossRef](#)] [[PubMed](#)]
3. Ficiarà, E.; Munir, Z.; Boschi, S.; Caligiuri, M.E.; Guiot, C. Alteration of Iron Concentration in Alzheimer’s Disease as a Possible Diagnostic Biomarker Unveiling Ferroptosis. *Int. J. Mol. Sci.* **2021**, *22*, 4479. [[CrossRef](#)] [[PubMed](#)]
4. Howard, C.M.; Jain, S.; Cook, A.D.; Packard, L.E.; Mullin, H.A.; Chen, N.; Liu, C.; Song, A.W.; Madden, D.J. Cortical Iron Mediates Age-Related Decline in Fluid Cognition. *Hum. Brain Mapp.* **2022**, *43*, 1047–1060. [[CrossRef](#)]
5. McCarthy, R.C.; Kosman, D.J. Iron Transport across the Blood-Brain Barrier: Development, Neurovascular Regulation and Cerebral Amyloid Angiopathy. *Cell. Mol. Life Sci.* **2015**, *72*, 709–727. [[CrossRef](#)]
6. Moos, T.; Morgan, E.H. Transferrin and Transferrin Receptor Function in Brain Barrier Systems. *Cell Mol. Neurobiol.* **2000**, *20*, 77–95. [[CrossRef](#)]
7. Zheng, W.; Aschner, M.; Ghersi-Egea, J.-F. Brain Barrier Systems: A New Frontier in Metal Neurotoxicological Research. *Toxicol. Appl. Pharmacol.* **2003**, *192*, 1–11. [[CrossRef](#)]
8. Zheng, W.; Monnot, A.D. Regulation of Brain Iron and Copper Homeostasis by Brain Barrier Systems: Implication in Neurodegenerative Diseases. *Pharmacol. Ther.* **2012**, *133*, 177–188. [[CrossRef](#)]
9. Bjorefeldt, A.; Illes, S.; Zetterberg, H.; Hanse, E. Neuromodulation via the Cerebrospinal Fluid: Insights from Recent in Vitro Studies. *Front. Neural. Circuits* **2018**, *12*, 5. [[CrossRef](#)]
10. Boespflug, E.L.; Iliff, J.J. The Emerging Relationship Between Interstitial Fluid-Cerebrospinal Fluid Exchange, Amyloid- $\beta$ , and Sleep. *Biol. Psychiatry* **2018**, *83*, 328–336. [[CrossRef](#)]
11. Holmes-Hampton, G.P.; Chakrabarti, M.; Cockrell, A.L.; McCormick, S.P.; Abbott, L.C.; Lindahl, L.S.; Lindahl, P.A. Changing Iron Content of the Mouse Brain during Development. *Metallomics* **2012**, *4*, 761–770. [[CrossRef](#)] [[PubMed](#)]
12. Chen, J.-H.; Singh, N.; Tay, H.; Walczyk, T. Imbalance of Iron Influx and Efflux Causes Brain Iron Accumulation over Time in the Healthy Adult Rat. *Metallomics* **2014**, *6*, 1417–1426. [[CrossRef](#)] [[PubMed](#)]
13. Lopes, T.J.; Luganskaja, T.; Vujić Spasić, M.; Hentze, M.W.; Muckenthaler, M.U.; Schümann, K.; Reich, J.G. Systems Analysis of Iron Metabolism: The Network of Iron Pools and Fluxes. *BMC Syst. Biol.* **2010**, *4*, 112. [[CrossRef](#)] [[PubMed](#)]
14. Berzuini, C.; Franzone, P.C.; Stefanelli, M.; Viganotti, C. Iron Kinetics: Modelling and Parameter Estimation in Normal and Anemic States. *Comput. Biomed. Res.* **1978**, *11*, 209–227. [[CrossRef](#)] [[PubMed](#)]
15. Pollycove, M.; Mortimer, R. The Quantitative Determination Of Iron Kinetics And Hemoglobin Synthesis In Human Subjects. *J. Clin. Invest.* **1961**, *40*, 753–782. [[CrossRef](#)]
16. Khan, A.I.; Liu, J.; Dutta, P. Iron Transport Kinetics through Blood-Brain Barrier Endothelial Cells. *Biochim. Biophys. Acta* **2018**, *1862*, 1168–1179. [[CrossRef](#)] [[PubMed](#)]
17. Ficiarà, E.; D’Agata, F.; Ansari, S.; Boschi, S.; Rainero, I.; Priano, L.; Cattaldo, S.; Abollino, O.; Cavalli, R.; Guiot, C. A Mathematical Model for the Evaluation of Iron Transport across the Blood-Cerebrospinal Fluid Barrier in Neurodegenerative Diseases. In Proceedings of the 2020 42nd Annual International Conference of the IEEE Engineering in Medicine Biology Society (EMBC), Montreal, QC, Canada, 20–24 July 2020; pp. 2270–2273.
18. Ficiarà, E.; D’Agata, F.; Cattaldo, S.; Priano, L.; Mauro, A.; Guiot, C. A Compartmental Model for the Iron Trafficking Across the Blood-Brain Barriers in Neurodegenerative Diseases. In Proceedings of the 2021 43rd Annual International Conference of the IEEE Engineering in Medicine Biology Society (EMBC), Virtual Conference, 1–5 November 2021; pp. 4200–4203.
19. Ficiarà, E.; Boschi, S.; Ansari, S.; D’Agata, F.; Abollino, O.; Caroppo, P.; Di Fede, G.; Indaco, A.; Rainero, I.; Guiot, C. Machine Learning Profiling of Alzheimer’s Disease Patients Based on Current Cerebrospinal Fluid Markers and Iron Content in Biofluids. *Front. Aging Neurosci.* **2021**, *13*. [[CrossRef](#)]
20. Kennedy, J.; Eberhart, R.C. Particle Swarm Optimization. *Proc. 1995 IEEE Int. Conf. Neural Netw.* **1995**, *1*, 1942–1948.

21. Pedersen, M.E.H.; Chipperfield, A.J. Simplifying Particle Swarm Optimization. *Appl. Soft Comput.* **2010**, *10*, 618–628. [[CrossRef](#)]
22. Shi, Y.; Eberhart, R.C. A Modified Particle Swarm Optimizer. *Proc. 1998 IEEE Int. Conf. Evol. Comput.* **1998**, *1*, 69–73.
23. Perracchione, E.; Stura, I. RBF Kernel Method and Its Applications to Clinical Data. *Dolomites Res. Notes Approx.* **2016**, *9*, 13–18.
24. Massa, P.; Perracchione, E.; Garbarino, S.; Battaglia, A.F.; Benvenuto, F.; Piana, M.; Hurford, G.; Krucker, S. Imaging from STIX Visibility Amplitudes. *Astron. Astrophys.* **2021**, *656*, A25. [[CrossRef](#)]
25. Wright, S.; Nocedal, J. Numerical Optimization. *Springer Sci.* **1999**, *35*, 67–68.
26. Stura, I.; Perracchione, E.; Migliaretti, G.; Cavallo, F. A New Numerical Method for Processing Longitudinal Data: Clinical Applications. *Epidemiol. Biostat. Public Health* **2018**, *15*. [[CrossRef](#)]
27. Zecca, L.; Youdim, M.B.H.; Riederer, P.; Connor, J.R.; Crichton, R.R. Iron, Brain Ageing and Neurodegenerative Disorders. *Nat. Rev. Neurosci.* **2004**, *5*, 863–873. [[CrossRef](#)]
28. Ficiarà, E.; Stura, I.; Guiot, C. Iron Deposition in Brain: Does Aging Matter? *Int. J. Mol. Sci.* **2022**, *23*, 10018. [[CrossRef](#)] [[PubMed](#)]
29. Pahnke, J.; Langer, O.; Krohn, M. Alzheimer's and ABC Transporters—New Opportunities for Diagnostics and Treatment. *Neurobiol. Dis.* **2014**, *72 Pt A*, 54–60. [[CrossRef](#)]